

# Precise Positioning of Nanoparticles on Surfaces Using Scanning Probe Lithography

Jayne C. Garno,<sup>†,‡</sup> Yiyun Yang,<sup>§</sup> Nabil A. Amro,<sup>†</sup> Sylvain Cruchon-Dupeyrat,<sup>‡,||</sup> Shaowei Chen,<sup>\*,§</sup> and Gang-Yu Liu<sup>\*,†</sup>

*Department of Chemistry, University of California, Davis, California 95616, Department of Chemistry, Wayne State University, Detroit, Michigan 48202, and Department of Chemistry and Biochemistry, Southern Illinois University, Carbondale, Illinois 62901*

*Received December 10, 2002; Revised Manuscript Received January 16, 2003*

## ABSTRACT

Two new methods have been developed to precisely position gold nanoparticles on surfaces. The surface-active nanoparticles have a shell of a mixed monolayer comprised of alkanethiol and alkanedithiol molecules to anchor particles to gold surfaces via sulfur–gold chemisorption. In the first method, regions of an alkanethiol self-assembled monolayer (SAM) are shaved by the AFM tip under high force in a solution containing nanoparticles. Nanoparticles then adsorb onto the exposed areas defined by the shaving track of the tip. In a second method, the AFM tip is coated with nanoparticles. Under low force, AFM images are acquired and the nanoparticles remain on the tip. When higher load is applied, areas of the SAM matrix are uncovered and nanoparticles are deposited following the scanning track of the AFM tip. Thus, the 3D positions of the nanoparticles are precisely controlled. The nanostructures are characterized *in situ* with the same tip at reduced load. Individual particles within the nanopatterns can be resolved by AFM. In both methods, the matrix SAM effectively resists the nonspecific binding of nanoparticles, and prevents lateral diffusion of nanoparticles. The high spatial precision offered by AFM lithography is advantageous for fabrication of nanoparticle-based nanodevices.

Metal nanoparticles exhibit size-dependent optical,<sup>1</sup> electronic,<sup>2,3</sup> and catalytic properties,<sup>4</sup> which have great potential for engineering new materials and sensors.<sup>5,6</sup> Prospective applications for nanoparticles include miniature electronic devices,<sup>7–9</sup> spin coatings,<sup>10</sup> and biosensing.<sup>11–14</sup> Prototype devices in molecular electronics, which incorporate gold nanoparticles as components, include single-electron transistors,<sup>8,15–17</sup> single-electron charging devices, photonic switches,<sup>18</sup> and quantum dots.<sup>19</sup> The 3D positions of nanoparticles on surfaces must be controlled precisely—hopefully at the level of individual particles. To make micro- and nanoscale devices functional, nanoparticles must be aligned precisely in nanowires<sup>20,21</sup> and nanoparticles must be positioned precisely at the gap of metal–insulator–metal junctions.<sup>22</sup>

Methods are continuously being developed and improved for directing the organization of metal nanoparticles into thin film layers,<sup>23,24</sup> nanocrystal arrays,<sup>25</sup> and superlattices.<sup>26</sup> Hexagonal ordering has been achieved using approaches such

as the Langmuir–Blodgett method.<sup>27,28</sup> Stepwise derivatization procedures have been used to form multilayered Au colloid films attached to amine-terminated thiols/Au(111).<sup>29</sup> These methods provide approaches for assembling nanoparticles into highly organized ensembles and layers for macro- and microapplications.

For applications involving micro- and nanodevices, lithographic approaches have been developed to position nanoparticles. For example, surfaces of micropatterned self-assembled monolayers (SAMs) produced by microcontact printing<sup>30–32</sup> and by photolithography<sup>30</sup> served as templates to guide nanoparticles into micropatterns. In these strategies, the selectivity of adsorption is dictated by the interactions between nanoparticles and surfaces. The feature sizes achieved thus far for these approaches are on the order of microns.

To reach nanometer precision, scanning probe lithography has been used to pattern nanoparticles. Iron oxide nanoparticles, 4–16 nm in diameter, were adsorbed onto patterned self-assembled monolayer (SAM) surfaces.<sup>33</sup> The patterned SAMs were produced using dip-pen nanolithography (DPN), an AFM-based method.<sup>34</sup> In another approach, metal nanoparticles were directly placed on surfaces by first depositing a small volume of solution containing nanoparticles using

\* To whom correspondence should be addressed. Tel: 530-754-9678; Fax: 530-752-8995; E-mail: liu@chem.ucdavis.edu

<sup>†</sup> University of California, Davis.

<sup>‡</sup> Wayne State University.

<sup>§</sup> Southern Illinois University.

<sup>||</sup> Present address: NanoInk, Inc., 1436 W. Randolph St. #402, Chicago, IL 60607

DPN, then letting the solvent evaporate.<sup>35</sup> These DPN-based approaches further miniaturized fabrication in comparison to photolithography and microcontact printing. However, lateral dispersion was present, thus compromising the lateral precision.<sup>36</sup>

Lateral dispersion was eliminated by using SAMs as resists. AFM tips were used to remove siloxane molecules exposing SiO<sub>2</sub> for subsequent amine functionalization.<sup>37</sup> Citrate stabilized gold nanoparticles then adsorbed onto amine-terminated patterns. Silica was typically elevated above the surrounding resist layer. The height of the silica depends on the degree of oxidation. The lateral dimension was precisely controlled, however, the perpendicular dimension was difficult to regulate due to the difficulties of controlling tip-induced oxidation.<sup>37</sup>

In this article, we introduce two approaches in which 3D positioning can be controlled with nanometer precision. Both methods can precisely position nanoparticles within alkanethiol resists using AFM-based lithography. The attachment occurs by chemisorption to the substrate via multiple S–Au linkages, since the nanoparticles are composed of a gold core and an outer shell of mixed thiols.<sup>38</sup> Sulfur–gold chemisorption defines the perpendicular precision. The surrounding matrix of methyl-terminated alkanethiols effectively resists the nonspecific binding of nanoparticles and prevents lateral diffusion.

Gold (Alfa Aesar, 99.99% Ward Hill, MA) was deposited onto freshly cleaved mica substrates (clear ruby muscovite mica, S&J Trading Company, New York, NY) according to a previously reported procedure.<sup>39</sup> The substrates were preheated to 325 °C in a high vacuum evaporator (Denton Vacuum Inc., Moorestown, NJ, model DV502-A) at  $2 \times 10^{-7}$  Torr. The evaporation rate was maintained at 3 Å/s during gold deposition. The final film thickness ranged between 150 and 200 nm. After deposition, the temperature was maintained at 325 °C for an additional 15 min for annealing. After removing the films from the UHV chamber, pieces of glass were affixed to the films using Epotek 377 (Epoxy Technologies, Inc., Billerica, MA) and cured for 2 h at 150 °C. Films of gold glued to glass in this fashion can be stored at room temperature for several months. Stripping the glass pieces from the mica produces clean Au(111) surfaces, with flat areas as large as  $300 \times 300$  nm<sup>2</sup> and a mean roughness as small as 2–5 Å, according to AFM measurements.

Alkanethiols were available commercially and used as received: 1-decanethiol (HS(CH<sub>2</sub>)<sub>9</sub>CH<sub>3</sub>, 96% purity) and 1-dodecanethiol (HS(CH<sub>2</sub>)<sub>11</sub>CH<sub>3</sub>, 96% purity) from Aldrich; *n*-hexadecylmercaptan (HS(CH<sub>2</sub>)<sub>15</sub>CH<sub>3</sub>, 92%) from Pfaltz and Bauer; *n*-hexadecane (99%) from Sigma; *sec*-butanol (99.7%) from Fisher Chemicals. SAMs were prepared by immersing freshly stripped pieces of ultraflat gold on glass into the desired thiol solution. Typically the substrates were placed into 0.1 mM solutions of thiol in *sec*-butanol for at least 24 h to ensure the formation of a complete, stable monolayer. The SAMs were removed from solution and rinsed copiously with *sec*-butanol and ethanol before AFM imaging.

Encapsulated gold nanoparticles with alkanethiol shells have been modified via place-exchange reactions to include

an outer shell of mixed thiol composition.<sup>38</sup> Typically, particles protected with only dithiol ligands aggregate readily in solution, due to disulfide cross-linking between particles. A stable dispersion has been achieved using nanoparticles with a mixed monolayer shell consisting of both thiol and methyl terminal groups. The thiol groups on the nanoparticle surfaces offer an advantage for chemisorptive attachment to gold surfaces. The synthesis of surface-active nanoparticles has been described in detail previously.<sup>38</sup> Briefly, alkanethiolate-protected gold nanoparticles were first synthesized by using the biphasic Brust route.<sup>40</sup> Then, multiple copies of alkanedithiols were exchanged into the protecting monolayers of hexanethiolate-protected gold nanoparticles dissolved in hexane, rendering the resulting particles surface-active, with free thiols on the outer peripheral surface. Excess dithiols and displaced thiols were removed by repetitive methanol extractions from the exchange (hexane) solution. These surface-active nanoparticles were kept in hexane or decane solutions to minimize particle cross-linking. They could then be used for surface assembling and nanofabrication.

A home-constructed atomic force microscope (AFM) with the optical-beam deflection configuration was used for this study.<sup>41,42</sup> Samples are placed on a segmented piezo-tube stage for translation, and the cantilever is mounted in a fixed position. A laser is focused on the back of the cantilever and deflected to a four-segment photosensitive detector, which monitors the vertical deflection and lateral twisting of the cantilever as the sample is rastered against the tip. This design enables the simultaneous acquisition of topography, frictional force, and elasticity images. The electronic controllers and software are from RHK Technology (Troy, MI). Images were acquired in *sec*-butanol or in hexadecane. The AFM scanner was calibrated using commercial calibration grids, with a periodicity of 3.0 μm and heights of 22.0, 100, and 485 nm, respectively (NT-MDT, Moscow, Russia). Commercially available Si<sub>3</sub>N<sub>4</sub> cantilevers were used for imaging, with force constants of 0.1 N/m (Microsharpened cantilever, Thermo Microscopes, Sunnyvale, CA). The imaging force was typically less than 0.5 nN.

A contact-resonance imaging (CRI) method was used to improve topographic image contrast by minimizing tip–surface interactions.<sup>43</sup> With CRI, the tip remains in contact with the surface while the sample is sinusoidally modulated at a resonance frequency of the tip–sample contact. This mode is effective for improving the imaging contrast both in liquid media and under ambient conditions, using standard commercially available soft cantilevers.

The AFM controller was interfaced with a programmable vector scanning module (VSCAN, RHK Technology, Inc.) to enable automated scanning probe lithography.<sup>44</sup> Sets of programmed motions were written and compiled into lithography scripts to create the desired surface arrangements of nanopatterns. Scripts were written that controlled the length, direction, speed, and the applied force of the scanning motion during lithography. Automated scanning probe lithography enabled the rapid fabrication of multiple nanopatterns in well-

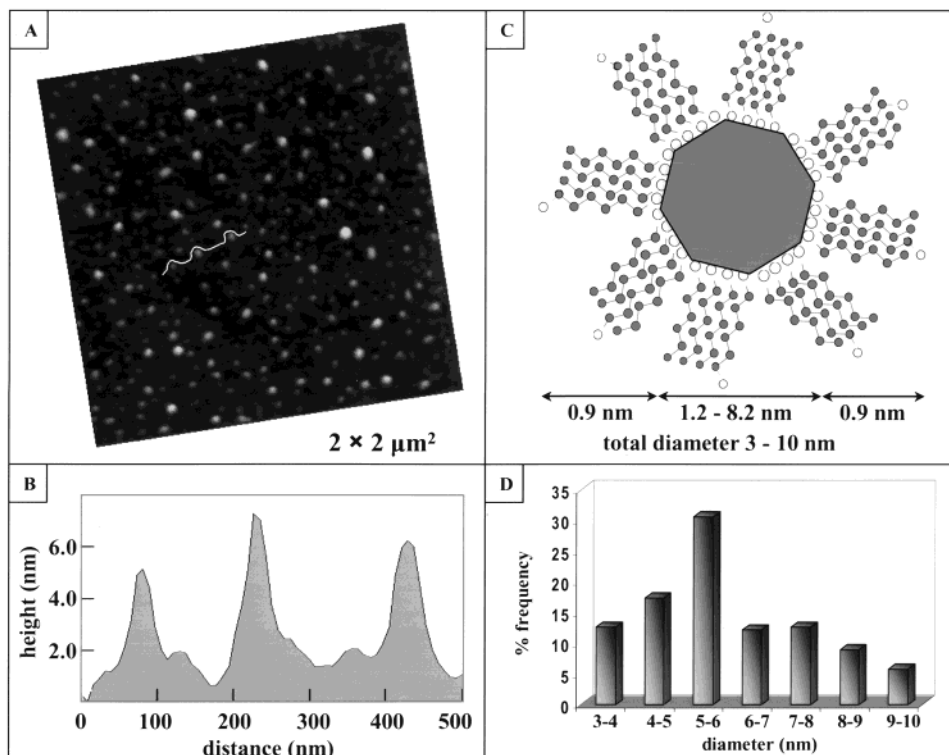


**Figure 1.** Characterization of nanoparticles chemisorbed on Au(111). (A) A topographic image ( $2 \times 2 \mu\text{m}^2$ ). (B) Corresponding cursor profile for A. (C) Schematic diagram of the cross-sectional view of the thiol-passivated nanoparticles. (D) Histogram of the heights measured for 190 nanoparticles.

controlled, repeatable conditions, as well as the production of arrays of nanostructures.

For size assessment, nanoparticles were immobilized on a clean gold surface via thiol chemisorption on gold. The desired surface coverage was achieved by adjusting both the concentration and immersion time. In the AFM topograph shown in Figure 1A, the Au(111) substrate was immersed directly in a 0.005 mg/mL solution of nanoparticles in hexadecane for 8 h. The cursor plot of Figure 1B indicates the heights of three selected nanoparticles as  $4.7 \pm 0.2$  nm,  $7.0 \pm 0.2$  nm, and  $5.6 \pm 0.2$  nm. The lateral dimensions of nanoparticles measured in the AFM topograph include AFM tip convolution.<sup>45,46</sup> Therefore, to ensure accurate size determination, only height measurements were used for data analysis. The schematic in Figure 1C depicts a cross-sectional view of thiol-modified nanocrystals, for which the overall and specific dimensions of the metal core and the length of the thiol shell are clearly illustrated. According to AFM measurements, the overall diameters range from 3 to 10 nm, thus the metal cores correspondingly range in size from 1.2 to 8.2 nm. The size distribution is displayed in Figure 1D, based on measurements of 190 particles imaged within various regions of the same sample. The histogram shows that 85% of the particles range between 4 and 8 nm in diameter. The average value was 6.1 nm.

A zoom-in view ( $1 \times 1 \mu\text{m}^2$ ) is shown in Figure 2, where simultaneously acquired topographic and amplitude images are displayed side-by-side. The amplitude image was acquired with the sample vibrating at a resonance frequency of the AFM tip-gold surface contact.<sup>47</sup> The resonance

frequency was used to enhance the image contrast for amplitude and phase signals. While the particle size can be extracted from the AFM topographs, as discussed previously, corresponding amplitude images provide information regarding the tip-sample interactions. For particles without a thiol shell, homogeneous contrast was observed in amplitude and phase images. With core-shell nanoparticles, amplitude images taken at resonances were sufficiently sensitive to reveal a dark contrast when the tip was mostly in contact with the thiol shell (see Figure 2C). When the tip is on top of the particle, the resonance amplitude is highly damped (dark), because tip-thiol molecule interactions are sufficiently different from that in the tip-Au contact. This force modulation approach provides an effective means to identify the presence of core-shell particles.

Two methods were developed for precisely positioning nanoparticles on gold surfaces. The first method (Figure 3A) combines nanoshaving of a matrix SAM with subsequent adsorption of nanoparticles onto the exposed areas of the substrate. The main steps are as follows: first, the sample is characterized by AFM under low force in a solution containing nanoparticles. A relatively flat area with few defects is typically chosen for fabrication. In the second step, nanofabrication is accomplished by shaving areas of a methyl-terminated alkanethiol SAM matrix under high force. The AFM tip is used as a fabrication tool, to plow a furrow within a field of SAM matrix. Nanoparticles attach selectively on the uncovered areas of the gold surface, via sulfur-gold chemisorption. In the final step, the nanoparticles within the nanopatterns are imaged using the same AFM tip.

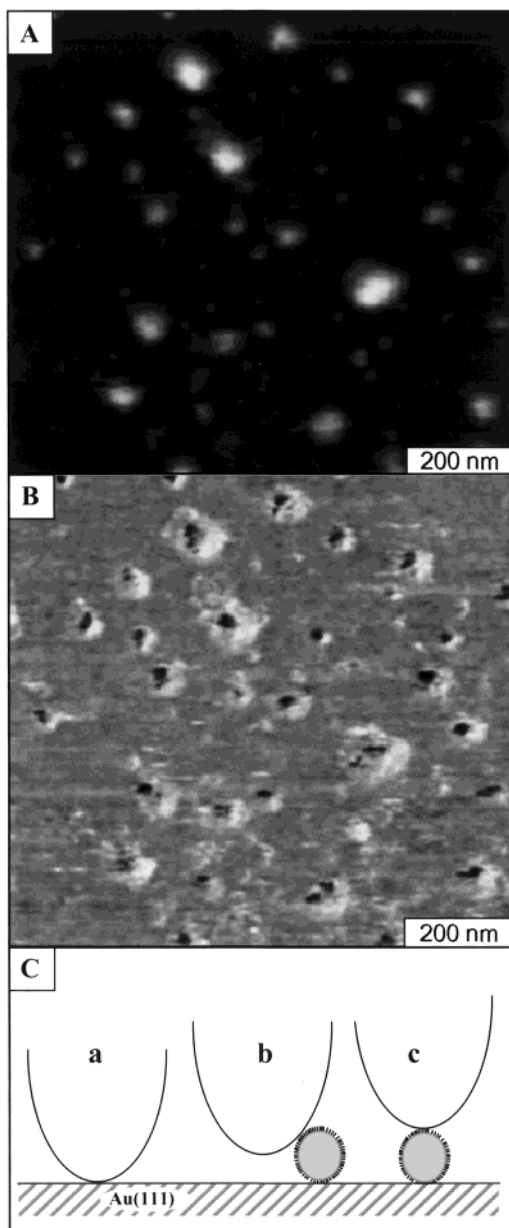


**Figure 2.** AFM topographic (A) and amplitude (B) images acquired at a resonance frequency of 38 kHz and modulation amplitude of 74 Å. (C) Schematic diagram illustrating three important tip-surface contacts: (a) tip-gold substrate, (b) tip-substrate/tip-edge of particles, and (c) tip-top of particle.

The second method for patterning nanoparticles uses NanoPen Reader and Writer, NPRW,<sup>48</sup> and can be accomplished either in air or in a particle-immiscible solvent such as *sec*-butanol. The procedure is illustrated in Figure 3B. The mixed shell of the nanoparticles containing free thiol groups are suitable for coating thiophilic silicon nitride AFM tips. Droplets of nanoparticle solution are applied directly to an inverted AFM tip in 0.1  $\mu\text{L}$  increments and allowed to dry. A stereomicroscope is used to carefully monitor the deposition of liquids from a microliter syringe. After deposition, the solvent evaporates rapidly. Within minutes the tip is ready to use as a brush to paint nanopatterns. The next steps of nanofabrication are identical as for NPRW using thiol molecules.<sup>48</sup> The alkanethiol SAM

resist is first characterized under low force. An area is chosen for fabrication, and higher force is applied to push the tip through the matrix SAM to deposit nanoparticles onto the Au(111) surface. Matrix molecules under the tip are scraped away at high force and displaced with the scanning motion of the tip to other areas of the sample or dissolved into the surrounding liquid. Nanoparticle “paint” from the tip is deposited onto the uncovered areas of the substrate under high force, following the scanning track of the AFM tip. Returning to lower force for imaging, the newly generated nanopattern can be characterized. As with NPRW, a single AFM tip is used for the steps of characterization and fabrication. Both methods in principle can precisely position nanoparticles on surfaces. Methyl-terminated SAM matrices prevent adsorption of gold nanoparticles and eliminate lateral diffusion. The shell of mixed thiols determines the perpendicular position.

An example of the results from nanoshaving and selective adsorption is shown in Figure 4. The sample was immersed in a 0.01 mg/mL solution of nanoparticles in hexadecane for the duration of the experiment. Figure 4A shows a nanoshaved rectangular area, surrounded by a decanethiol matrix. Fabrication was accomplished with a single scan of the  $150 \times 300 \text{ nm}^2$  region. Decanethiol molecules were not removed completely with one scan; however, the removal of most adsorbates within the frame is clearly evident in Figure 4A. Several Au steps and a deep crack are visible surrounding the pattern, which serve as landmarks for in situ imaging. After 12 h, the patterned area filled with nanoparticles, as shown in Figure 4B. A cursor plot within the hole measures a depth of  $1.2 \pm 0.2 \text{ nm}$ , which is slightly smaller than the expected thickness of a decanethiol SAM (1.5 nm). This corresponds to incomplete removal of thiol molecules within the fabricated areas, shown by the gray shaded area of the combined cursor plot of Figure 4C. The incomplete removal of matrix thiol molecules does not seem to prevent adsorption of nanoparticles, as dithiols within the shell can reach areas of bare gold and anchor the particles on the surface. Cursor measurements of the nanostructures shown in Figure 4B show that nanoparticles under measurement exhibit a height of  $2.3 \pm 0.3 \text{ nm}$  above the matrix, thus the overall nanoparticle diameter measures  $3.8 \pm 0.3 \text{ nm}$ . Systematic data analysis shows that the nanoparticle sizes within the nanopattern range from 3 to 5 nm in diameter. The height measurements are consistent with a single layer of nanoparticles. Additionally, individual nanoparticles can be resolved, despite the effects of tip convolution. For the  $150 \times 300 \text{ nm}^2$  region shown in Figure 4B, approximately 51 nanoparticles are packed within the nanopattern.

In contrast to nanografting of thiol SAMs,<sup>49</sup> adsorption of nanoparticles is slower. There are orders of magnitude differences between the size of thiol molecules and nanoparticles, which contribute to a much lower mobility for nanoparticles. Also, there is a very large difference in concentration for the experimental conditions. For a given 1 mL volume, a typical solution of hexanethiol (0.1 mM) would contain approximately  $10^{20}$  hexanethiol molecules for nanografting, as compared to  $10^{13}$  nanoparticles for a 0.01

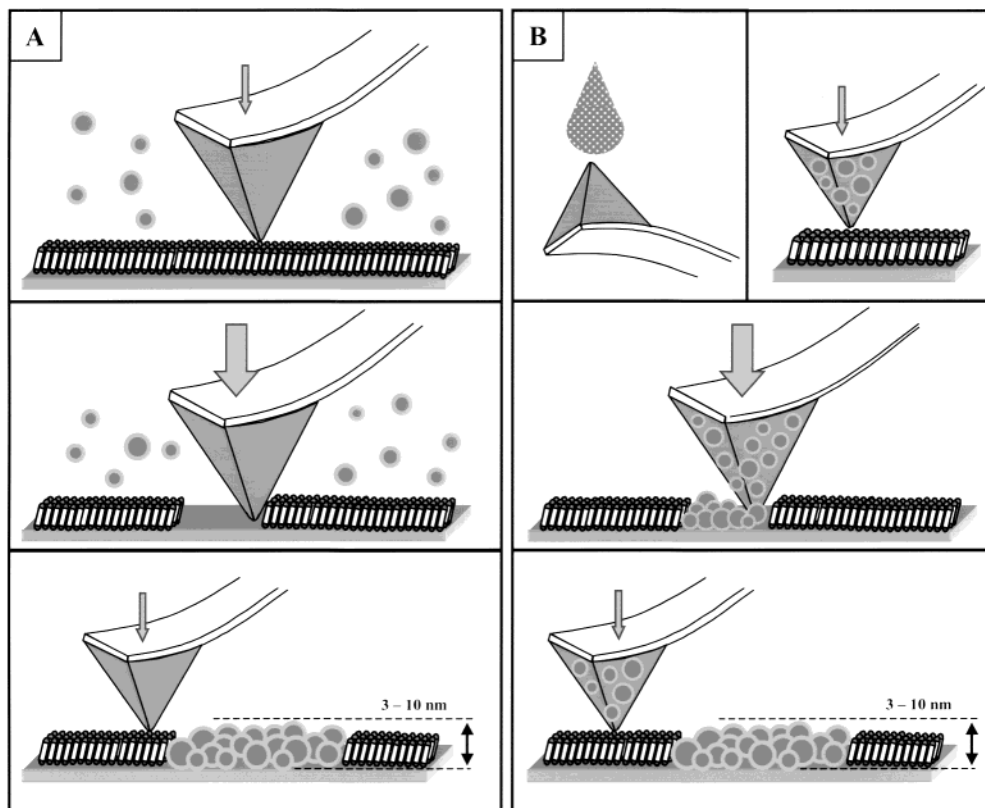


**Figure 3.** Two methods for positioning nanoparticles via scanning probe lithography. (A) Nanoshaving followed by selective adsorption of nanoparticles. (B) Removal of SAM resist followed by deposition of mixed-shell nanoparticles from the tip (NPRW).

mg/mL solution of nanoparticles—a 10 million-fold difference. Thus, a slower diffusion is expected and observed for nanoparticle systems. For nanoparticle concentrations of 0.02, 0.01, and 0.005 mg/mL, adsorption over areas of hundreds of nanometers was completed after 10, 16, and 30 h, respectively.

Nanoparticle adsorption onto nanoshaved areas of alkanethiol SAMs provides one approach for positioning nanoparticles, with advantages of being highly localized and selective. Automated scanning probe lithography enables production of arrays of nanostructures with designed geometries and dimensions. As a preliminary experiment, arrays of nanopatterns were produced under a solution of 0.02 mg/mL of nanoparticles. These include  $3 \times 3$  arrays of 100 nm nanostructures of core-shell nanoparticles within a dodecanethiol matrix SAM.<sup>50</sup>

For DPN<sup>34</sup> and NPRW,<sup>48</sup> typically the procedure to coat the AFM tip (pen) with thiols (ink) includes either dipping or submerging a tip into a solution containing the thiol molecules of interest. However, for nanoparticle solutions, the tip coating procedure needed to be modified for two reasons. First, with an immersion or dipping procedure, the back of the cantilever became densely covered with nanoparticles, because gold is commonly used as the reflective coating. The layers of nanoparticles greatly reduced the reflection intensity of the laser beam, thus making imaging difficult. Second, when using a dipping process to only immerse the apex of the tip in solution, very few particles deposited onto the tip and thus did not provide a sufficient nanoparticle coating. For effective NPRW, multiple small

drops of nanoparticle solution were deposited onto an inverted tip. The solvent evaporated rapidly to generate a sufficient amount of nanoparticles applied only to the desired areas at the apex of the tip, instead of covering the back of the cantilever.

Successful examples of nanostructures of gold nanoparticles produced using NPRW are shown in Figure 5. An accumulative volume of  $5 \mu\text{L}$  of nanoparticles in hexane (0.10 mg/mL) was deposited onto an AFM tip in  $\mu\text{L}$  increments with a glass syringe and allowed to evaporate. The tip was then used to image a decanethiol SAM in *sec*-butanol, revealing fine structural details of the matrix SAM, such as defects. When higher force was applied to the tip, and also using slow scanning rates (approximately 200 nm/s), nanoparticles from the tip were transferred to the substrate following the writing track of the AFM tip. After the fabrication step, the force was reduced for characterizing the feature in situ. Nanoparticles were positioned within a  $150 \times 450 \text{ nm}^2$  rectangle as shown in Figure 5A. The height of the pattern ranged from 2.5 to 3.5 nm above the decanethiol matrix (Figure 5B), therefore the size of the particles ranged from 4.0 to 5.0 nm. It might be expected that using coated AFM tips would compromise the AFM imaging resolution; however, as shown in Figure 5A, the sacrifice in resolution is not significant. Steps of gold terraces and individual nanoparticles can still be resolved.

There are approximately 45 nanoparticles visible within the  $150 \times 450 \text{ nm}^2$  rectangular nanopattern in Figure 5A, which is far fewer than for a densely packed layer. Within a single experiment, multiple patterns with accumulated areas

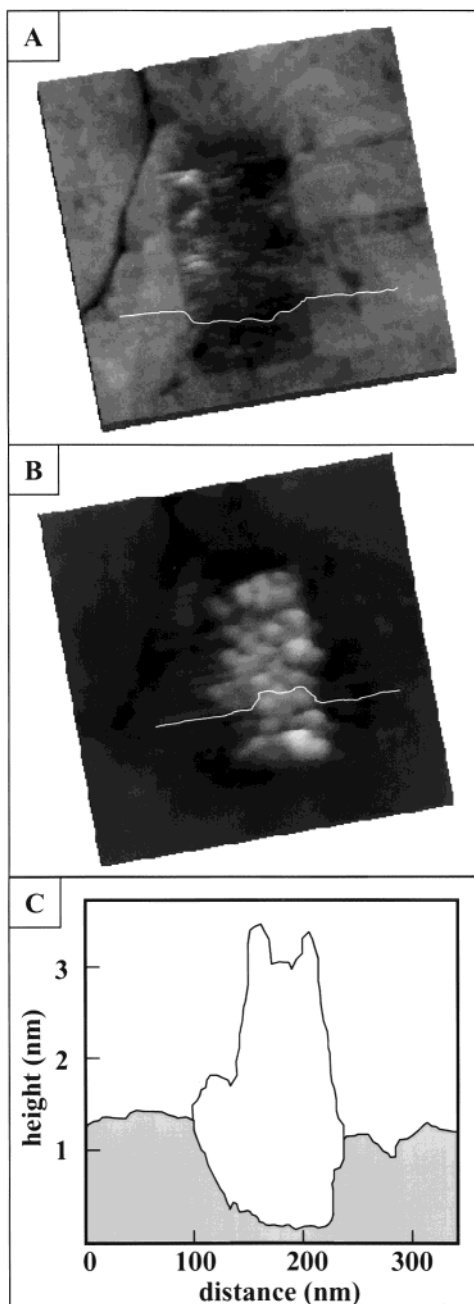


**Figure 4.** Positioning nanoparticles via nanoshaving and subsequent selective adsorption. (A) A  $150 \times 300 \text{ nm}^2$  area of thiol SAMs were shaved within a decanethiol matrix. (B) Same area imaged after 12 h immersion in 0.01 mg/mL nanoparticle solution. Nanoparticles attached selectively to the shaved areas. (C) A combined plot of the cursors indicated in A and B, the gray area indicates undisturbed matrix SAM, the white area indicates the area where nanoparticles attached.

of  $10^5 \text{ nm}^2$  were constructed without depleting the tip coating of nanoparticles. An advantage of this method is the versatility of working in various environments, such as ambient and liquid media. High selectivity was also observed, since nanoparticles do not deposit on areas of the surface unless higher force is applied. Since particles are localized on the AFM tips, slow diffusion rate is no longer an issue. The nanopatterning and characterization steps are very rapid; both steps are completed within a time frame of only 5–6 min.

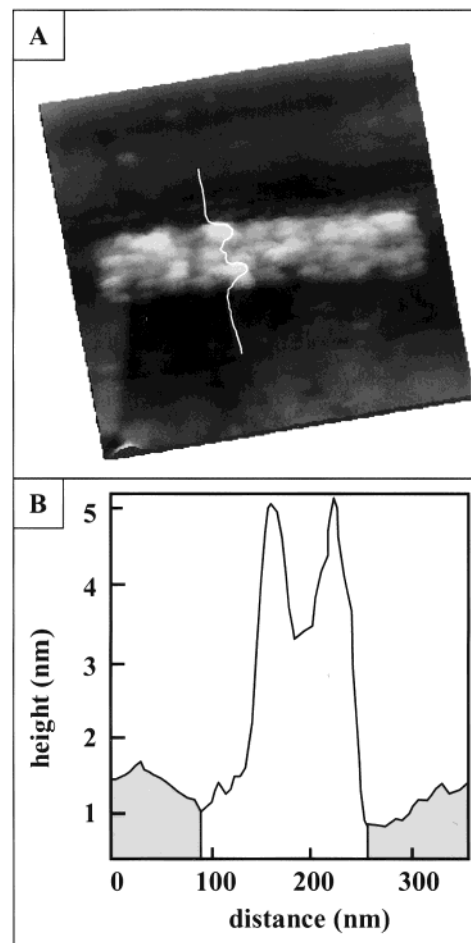


**Figure 5.** Positioning nanoparticles using NPRW. (A) AFM topograph ( $550 \times 550 \text{ nm}^2$ ) of a decanethiol SAM, where a  $150 \times 450 \text{ nm}^2$  rectangle of thiol-modified gold nanoparticles were placed with nanometer precision. (B) Corresponding cursor profile for A.

Nanoparticles can be positioned precisely on surfaces using AFM-based lithography. Two AFM-based nanopatterning methods were successfully demonstrated: nanoshaving followed by selective adsorption and NPRW. The nanoparticles which were used have a 1.2–8.2 nm gold core, covered by a mixed shell of alkanethiol and alkanedithiol molecules. Dithiol molecules serve as anchors to attach particles to surfaces. Surfaces are modified with SAMs to prevent lateral diffusion and nonselective adsorption of core–shell particles. These new methods prove to have nanometer precision for placing nanoparticles on surfaces. Only single layers of nanoparticles are observed. Nanopatterning can be achieved under ambient conditions, in aqueous solutions, or other solvents. The results are characterized in situ. Individual nanoparticles within the patterns can be resolved using AFM. Further work is in progress to resolve the nonspherical shape of core metal nanocrystals and molecular packing within the shells. If dithiol molecules can be selectively placed on specific crystalline faces, orientational specific immobilization would be possible. We anticipate that the results reported here will provide new approaches for nanoparticle-based electronic devices.

**Acknowledgment.** The authors thank University of California, Davis and the National Science Foundation (IGERT-970952 and IGERT-9972741) for financial support. Work at SIU was supported by the National Science Foundation (CAREER Award CHE-0092760) and the ACS Petroleum Research Fund (type G). S.C. is a Cottrell Scholar of Research Corp. We also acknowledge helpful discussions with William Price, Maozi Liu, Guohua Yang, James Benigna, and Candace Shepherd.

## References

- (1) Schmitt, J.; Machtle, P.; Eck, D.; Möhwald, H.; Helm, C. A. *Langmuir* **1999**, *15*, 3256–3266.
- (2) Brust, M.; Bethell, D.; Kiely, C. J.; Schiffrin, D. J. *Langmuir* **1998**, *14*, 5425–5429.
- (3) McConnell, W. P.; Novak, J. P.; Brousseau, L. C., III; Fuierer, R. R.; Tenent, R. C.; Feldheim, D. L. *J. Phys. Chem. B* **2000**, *104*, 8925–8930.
- (4) Johnson, B. F. G. *Coord. Chem. Rev.* **1999**, *190–192*, 1269–1285.
- (5) Fendler, J. H. *Chem. Mater.* **1996**, *8*, 1616–1624.
- (6) Shipway, A. N.; Katz, E.; Willner, I. *ChemPhysChem* **2000**, *1*, 18–52.
- (7) Ogawa, T.; Kobayashi, K.; Masuda, G.; Takase, T.; Maeda, S. *Thin Solid Films* **2001**, *393*, 374–378.
- (8) Junno, T.; Magnusson, M. H.; Carlsson, S.-B.; Deppert, K.; J.-O., M.; Montelius, L.; Samuelson, L. *Microelectron. Eng.* **1999**, *47*, 179–183.
- (9) Simon, U. *Adv. Mater.* **1998**, *10*, 1487–1492.
- (10) Cavicchi, R. E.; Walton, R. M.; Aquino-Class, M.; Allen, J. D.; Panchapakesan, B. *Sens. Actuators B* **2001**, *77*, 145–154.
- (11) Cai, H.; Xu, C.; He, P.; Y., F. *J. Electroanal. Chem.* **2001**, *510*, 78–85.
- (12) Demers, L. M.; Mirkin, C. A.; Mucic, R. C.; Reynolds, I., R. A.; Letsinger, R. L.; Elghanian, R.; Viswanadham, G. *Anal. Chem.* **2000**, *72*, 5535–5541.
- (13) Lazarides, A. A.; Kelly, K. L.; Jensen, T. R.; Schatz, G. C. *J. Mol. Struct.* **2000**, *529*, 59–63.
- (14) Kharitonov, A. B.; Shipway, A. N.; Willner, I. *Anal. Chem.* **1999**, *71*, 5441–5443.
- (15) Klein, D. L.; Roth, R.; Lim, A. K. L.; Alivisatos, A. P.; McEuen, P. L. *Nature* **1997**, *389*, 699–701.
- (16) Sato, T.; Ahmed, H.; Brown, D.; Johnson, B. F. G. *J. Appl. Phys.* **1997**, *82*, 696–701.
- (17) Thelander, C.; Magnusson, M. H.; Deppert, K.; Samuelson, L.; Poulsen, P. R.; Nygard, J.; Borggreen, J. *Appl. Phys. Lett.* **2001**, *79*, 2106–2108.
- (18) De, S.; Pal, A.; Pal, T. *Langmuir* **2000**, *16*, 6856–6861.
- (19) Baum, T.; Bethell, D.; Brust, M.; Schiffrin, D. J. *Langmuir* **1999**, *15*, 866–871.
- (20) Wyrwa, D.; Beyer, N.; Schmid, G. *Nano Lett.* **2002**, *2*, 419–421.
- (21) Chung, S.-W.; Markovic, G.; Heath, J. R. *J. Phys. Chem. B* **1998**, *102*, 6685–6687.
- (22) Feldheim, D. L.; Keating, C. D. *Chem. Soc. Rev.* **1998**, *27*, 1–12.
- (23) Grabar, K. C.; Allison, K. J.; Baker, B. E.; Bright, R. M.; Brown, K. R.; Freeman, R. G.; Fox, A. P.; Keating, C. D.; Musick, M. D.; Natan, M. *Langmuir* **1996**, *12*, 2353–2361.
- (24) Ramachandra Rao, C. N.; Kulkarni, G. U.; Thomas, J.; Edwards, P. P. *Chem. Soc. Rev.* **2000**, *29*, 27–35.
- (25) Hartmann, E.; Marquardt, P.; Ditterich, J.; Radojkovic, P.; Steinberger, H. *Appl. Surf. Sci.* **1996**, *107*, 197–202.
- (26) Martin, J. E.; Wilcoxon, J. P.; Odinek, J.; Provencio, P. *J. Phys. Chem. B* **2000**, *104*, 9475–9486.
- (27) Chen, S. *Langmuir* **2001**, *17*, 2878–2884.
- (28) Chen, X. Y.; Li, J. R.; Jiang, L. *Nanotechnology* **2000**, *11*, 108–111.
- (29) Musick, M. D.; Pena, D. J.; Botsko, S. L.; McEvoy, T. M.; Richardson, J. N.; Natan, M. J. *Langmuir* **1999**, *15*, 844–850.
- (30) Liu, J.-F.; Zhang, L.-G.; Gu, N.; Ren, J.-Y.; Wu, Y.-P.; Lu, Z.-H.; Mao, P. S.; Chen, D.-Y. *Thin Solid Films* **1998**, *327–329*, 176–179.
- (31) Liu, J.; Lee, T.; Janes, D. B.; Walsh, B. L.; Melloch, M. R.; Woodall, J. M.; Reifenger, R.; Andres, R. P. *Appl. Phys. Lett.* **2000**, *77*, 373–375.
- (32) He, H. X.; Zhang, H.; Li, Q. G.; Zhu, T.; Li, S. F. Y.; Liu, Z. F. *Langmuir* **2000**, *16*, 3846–3851.
- (33) Liu, X.; Fu, L.; Hong, S.; Dravid, V. P.; Mirkin, C. A. *Adv. Mater.* **2002**, *14*, 231–234.
- (34) Hong, S. H.; Zhu, J.; Mirkin, C. A. *Science* **1999**, *286*, 523–525.
- (35) Ali, M. B.; Ondarcuhu, T.; Brust, M.; Joachim, C. *Langmuir* **2002**, *18*, 872–876.
- (36) Piner, R. D.; Zhu, J.; Xu, F.; Hong, S. H.; Mirkin, C. A. *Science* **1999**, *283*, 661–663.
- (37) Zheng, J.; Zhu, Z.; Chen, H.; Liu, Z. *Langmuir* **2000**, *16*, 4409–4412.
- (38) Templeton, A. C.; Hostetler, M. J.; Warmoth, E. K.; Chen, S.; Hartshorne, C. M.; Krishnamurthy, V. M.; Forbes, M. D. E.; Murray, R. W. *J. Am. Chem. Soc.* **1998**, *120*, 4548–4849.
- (39) Wagner, P.; Hegner, M.; Guntherodt, H.-J.; Semenza, G. *Langmuir* **1995**, *11*, 3867–3875.
- (40) Brust, M.; Walker, M.; Bethell, D.; Schiffrin, D. J.; Whyman, R. J. *Am. Chem. Soc.* **1994**, *116*, 1–802.
- (41) Kolbe, W. F.; Ogletree, D. F.; Salmeron, M. B. *Ultramicroscopy* **1992**, *42*, 1113–1117.
- (42) Liu, G.-Y.; Fenter, P.; Chidsey, C. E. D.; Ogletree, D. F.; Eisenberger, P.; Salmeron, M. J. *Chem. Phys.* **1994**, *101*, 4301–4306.
- (43) Wadu-Mesthrige, K.; Amro, N.; Garno, J. C.; Cruchon-Dupeyrat, S.; Liu, G.-Y. *Appl. Surf. Sci.* **2001**, *175–176*, 391–398.
- (44) Cruchon-Dupeyrat, S.; Porthun, S.; Liu, G.-Y. *Appl. Surf. Sci.* **2001**, *175–176*, 636–642.
- (45) Schwarz, U. D.; Haefke, H.; Reimann, P.; Guntherodt, H.-J. *J. Microsc.* **1994**, *173*, 183–197.
- (46) Ramirez-Aguilar, K. A.; Rowlen, K. L. *Langmuir* **1998**, *14*, 2562–2566.
- (47) Jourdan, J. S.; Cruchon-Dupeyrat, S. J.; Huang, Y.; Kuo, P. K.; Liu, G.-Y. *Langmuir* **1999**, *15*, 6495–6504.
- (48) Amro, N. A.; Xu, S.; Liu, G.-Y. *Langmuir* **2000**, *16*, 3006–3009.
- (49) Xu, S.; Miller, S.; Laibinis, P. E.; Liu, G.-Y. *Langmuir* **1999**, *15*, 7244–7251.
- (50) Garno, J. C., Doctoral Dissertation, Chemistry Department; Wayne State University: Detroit, MI, 2002.

NL025934V